HHS Public Access

Author manuscript

Biomater Sci. Author manuscript; available in PMC 2022 May 04.

Published in final edited form as:

Biomater Sci. 2021 May 04; 9(9): 3284–3292. doi:10.1039/d0bm02100h.

Conformal Single Cell Hydrogel Coating with Electrically Induced Tip Streaming at an AC Cone

Zehao Pan[#,1], **Loan Bui**[#,2], **Vivek Yadav**[#,1], **Fei Fan**[2], **Hsueh-Chia Chang**[*,1,2,3], **Donny Hanjaya-Putra**[*,1,2,3]

[1]Department of Chemical and Biomolecular Engineering, University of Notre Dame, IN 46556, USA.

[2]Department of Aerospace and Mechanical Engineering, Bioengineering Graduate Program, University of Notre Dame, IN 46556, USA.

[3]Harper Cancer Research Institute, University of Notre Dame, IN 46556, USA.

Encapsulation of single cell in a thin hydrogel provides a more precise control of stem cell niches and better molecular transport. Despite recent advances in microfluidic technologies to allow encapsulation of single cell, existing methods rely on special crosslinking agent that are pre-coated on the cell surface and subject to the variation of the cell membrane, which limits their wide spread adoption. This work reports a high-throughput single-cell encapsulation method based on the “tip streaming” mode of alternating current (AC) electrospray, with encapsulation efficiencies over 80% after a tuned centrifugation. Dripping with multiple cells is curtailed due to gating by the sharp conic meniscus of the tip streaming mode that only allows one cell to be ejected at a time. Moreover, the method can be universally applied to both natural and synthetic hydrogels, as well as various cell types, including human multipotent mesenchymal stromal cells (hMSCs). Encapsulated hMSCs maintain good cell viability over an extended culture period and exhibit robust differentiation potential into osteoblasts and adipocytes. Collectively, electrically induced tip streaming enables high-throughput encapsulation of single cell with high efficiency and universality, which are applicable for various applications in cell therapy, pharmacokinetic study, and regenerative medicine.

Introduction

Single cell encapsulation in a micrometer-thick microgel is a new protective bioengineering strategy to increase the surface-to-volume ratio in cell encapsulation for cell therapy, 3D cell culture pharmacokinetic study, and tissue engineering. [1–3] Unlike the conventional approach where multiple cells are encapsulated in millimeter sized gel particle, the thin microgel

[*]Hsueh-Chia Chang (hchang@nd.edu) and Donny Hanjaya-Putra (dputra1@nd.edu) are co-corresponding authors.
[#]Zehao Pan, Loan Bui, and Vivek Yadav contributed equally to this work.

Author Contributions

Z.P., L.B., and V.Y., designed and performed research, analyzed data, and wrote the manuscript. F.F. performed research and analyzed hydrogels data. D.H-P and H.-C.C. conceived the ideas, designed the experiments, interpreted the data, and wrote the manuscript. All authors have approved the manuscript.

Conflicts of interest

The authors have declared that no conflict interest exists.

approach improves molecular transport and manipulability, which results in high survival and cell retention *in vivo.* [4–7] Thin microgels or conformal coatings not only allow rapid diffusion of oxygen, nutrients, and cellular waste, but also blocks immunoglobulin to mitigate innate immune response. [4,8] Moreover, the length scale of single cell laden microgels also helps avoid several unwanted outcomes including cell hypoxia, fibrotic capsule formation or infarction after transplantation. [9,10]

To produce a single cell encapsulation in a thin microgel, droplet microfluidics, vibrating jets, and inkjet technologies have to compromise between high throughput and microgels size. [11–14] Despite recent progress in droplet microfluidics for generating uniform micrometer-sized hydrogel droplets, [15–17] regular PDMS based microfluidic channels often cannot bear the high pumping pressure required to produce droplets similar to the size of the cell using the viscous hydrogel solution. This obstacle has recently been solved by pre-coating the cells with crosslinking agents (e.g. calcium carbonate nanoparticles) or using special crosslinking chemistry. [10,18] The controlled supply of crosslinking agents allows the sol-gel transition to happen within only a few micrometers around the cell, thus automatically eliminating the excess hydrogel around the cell and empty gel particles during extraction into the aqueous phase. [10] However, the adsorption rate of nanoparticles is highly influenced by the “stickiness” of the cell membrane, making the method subject to variation among different cell types and limiting the type of gels that can be used for cell encapsulation. An alternative approach is to use hydrodynamic method to create a jet thinner than the cell diameter so that Rayleigh instability will be induced around the cell forming a droplet containing a single cell with a thin gel layer. [15] Nonetheless, tuning of both the continuous and dispersed phase flow rates of the flow-focusing design is difficult and hence single-cell occupancy is difficult to achieve. Therefore, there is a need for a new technology that can produce robust conformal coating of single cell with high reproducibility and universality. Ideally, this generic technology does not require the assistance of a high-shear flow and does not depend on the cell and hydrogel-specific adsorbing crosslinking agents.

In this work, we propose a novel method for single cell encapsulation using an immersed alternating current (AC) electrospray that can not only produce predominantly single-cell thin-layered hydrogel bead, but also circumvent the cell- and hydrogel-specific adsorbing crosslinking agents. We demonstrate the universality of the method by using both natural (alginate and collagen) and synthetic (hyaluronic acid functionalized with norbornene groups, NorHA) hydrogels as encapsulation material. Alginate can be crosslinked using divalent cations (e.g., Ca^{2+} or Mg^{2+}), while collagen at neutral pH can be crosslinked simply by raising the temperature to 37°C. [19,20] On the other hand, synthetic NorHA hydrogels can be crosslinked using light-mediated thiol-norbornene chemistry. [21,22] To further demonstrate the universality of the technology across different cell types, breast cancer cell line MDA-MB-231 and human multipotent mesenchymal stromal cells (hMSCs) are used in all experiments as the model cell lines.

Experimental

Electrospray setup

The experiment uses laser-pulled glass micropipette with tip diameter of 30 μm (purchased from WPI, FL) and is described previously.[23,24] Briefly, the micropipette was housed in a plastic reservoir through a hole on its side wall (Figure 1A). The reservoir was attached on a glass substrate with indium tin oxide (ITO) layer (25 × 75 mm, SPI supplies, USA), which served as the counter electrode in the electrical system and was grounded. The alternating electric potential was generated from a function generator (Agilent) and amplified by a step-up transformer (Industrial Test Equipment, Port Washington, NY). The output potential was applied through an electrode inside the micropipette that is also in contact with the dispersed phase. All voltage mentioned in this report represents the root mean square voltage. A pressure regulator is used to control the pumping pressure on the aqueous phase. Images and videos were taken with a CCD camera (Retiga EXi, QImaging) connected to an inverted microscope.

Cell culture

Human Breast Cancer cells MDA-MB-231 were obtained from ATCC (HTB-26). Cells were thawed and expanded via serial passages. Cells were maintained at 37°C, 5% CO_2 in DMEM Medium (Cellgro, Corning) supplemented with 10% Fetal Bovine Serum and 1% antibiotics (penicillin and streptomycin).

Human Multipotent Mesenchymal Stromal Cells (hMSCs) from bone marrow were obtained from PromoCell (C-12974). Cells were thawed and expanded via serial passages. The cells were grown and maintained in Complete Mesenchymal Growth Medium-2 (PromoCell, C-28009) with additional 1% antibiotics (penicillin and streptomycin) at 37°C, 5% CO_2. Cells used for all experiments were between passage 4 and 7.

To induce osteogenic and adipogenic differentiation, hMSCs were switched to MSC Osteogenic Differentiation Medium (PromoCell, C-28013) and MSC Adipogenic Differentiation Medium 2 (PromoCell, C-28016), respectively. The cells were incubated in differentiation media for 7 days. All cell lines were routinely tested for mycoplasma contamination and were negative throughout this study.

Preparation of suspended cells

Cell suspension preparation for encapsulation was conducted based on standard procedure.[25] Briefly, to obtain suspended cells, adherent cells were detached by trypsin/EDTA (PromoCell, C-41020) for 5 min.

Centrifugation was performed (300g, 5min) to remove the trypsin-containing supernatant and to pellet the cells. Cells were then resuspended in PBS at a high concentration (1–2 million cells/ml). Prior to spraying, dispersed individual cells were achieved by pipetting the cell suspension multiple times followed by filtering it through a 40um mesh strainer.

Cell viability

Viable cells were visualized by staining the nuclei with 10μg/ml Hoechst 3342 (Invitrogen™, H3570) and cell membrane with 2 μM Calcein AM dye for 20 min at room temperature. Dead cells were determined as stained with 4μM Ethidium homodimer-1 (Invitrogen™, L3224) for 30 min at room temperature. Cell viability was quantified using fluorescent microscopy and ImageJ.

Quantification of differentiated cells

Osteogenic differentiation was detected by staining the cells with Alizarin Red S for extracellular calcium deposits. A 2% Alizarin Red S solution (Sigma-Aldrich, A5533) was prepared in dH_2O then filtered to remove debris. The solution pH of 4.1–4.3 was adjusted by hydrochloric acid or ammonium hydroxide. The cells were washed with PBS then fixed with Methanol 95% for 10 min and washed again with dH_2O. Staining was performed by incubating the cells with the Alizarin Red S solution for 30 min. After that, the cells were rinsed with dH_2O and kept in dH_2O for immediate imaging. The percentage of differentiated cells was calculated and compared between adherent cells and encapsulated cells. For further quantification of calcium deposits and comparison between control cells and differentiated cells, the absorbance at 520nm of each well was measured.

Adipogenic differentiation results in the formation of lipid droplets within the cells, which could be identified by staining with Oil Red O solution (BioVision, K580–24) following the protocol suggested by the manufacturer. Briefly the cells were washed with PBS and fixed with 10% Formalin for 30 min. The fixed cells were then stained with Oil Red O solution and the cell nuclei could be counterstained with Hematoxylin. As stained, the lipid droplets appeared in red color in microscopic images. Finally, Oil Red O stain can be extracted by isopropanol and the resulting solutions could be quantified by reading the absorbance at 492nm.

Encapsulation experiment

Alginate crosslinking was induced using the Ca-EDTA complex to deliver the Calcium ion for gelation. [26] Ca-EDTA complex was made by mixing equal molar of calcium chloride and ethylenediaminetetraacetic acid (EDTA) in HEPES-buffered DMEM (Sigma-Aldrich) solution at pH 7.4. 2% w/w Alginate (300kDa, low viscosity, Sigma) was then added into the solution and fully dissolved. Cells were added to the mixed solution before electrospray at a final concentration of 5×10^7 cells per ml. Crosslinking of the gel coating was achieved by adding final concentration of 0.01% acetic acid (Sigma) to the oil phase for 2 minutes. The cells were extracted to cell media through centrifugation after adding 10% w/w 1H,1H,2H,2H-perfluorooctanol (PFO). Staining of alginate was achieved by substituting FITC-labeled alginate (Creative PEGWorks, NC) for 20% of the original alginate solution.

Collagen I (Corning®, 354249) was first neutralized with 100mM HEPES (pH7.3 in 2X PBS) before mixing with cells at a final concentration of 2.5mg/ml. Staining of collagen was achieved by incubating with NHS-FITC (5/6-carboxyfluorescein succinimidyl ester, ThermoFisher) according to manufacturer's instruction on ice for two hours following instruction provided by the manufacturer. To prevent premature gelation of collagen, all the

preparation and encapsulation steps were performed with cooling using ice. Crosslinking of the collagen was achieved by incubating the water-in-oil emulsion at 37 °C for 30 minutes.

NorHA was synthesized using an established protocol. [21,22] NorHA gel precursor solution containing 1.2% NorHA with 0.8 ratio of dithiothreitol (DTT). Water soluble photoinitiator Lithium phenyl-2,4,6-trimethylbenzoylphosphinate (LAP) was used at 0.2% (w/v) unless otherwise stated and was purchased from Sigma-Aldrich. After collecting the cell laden microgel droplets in a microcentrifuge tube, OmniCure® Series 1500 was used for crosslinking the NorHA precursor solution for 5 seconds with UV exposure (10 mW/cm^2, 365 nm). To visualize the gel layer, 2mM of rhodamine-thiol dye (Kerafast, Boston, MA) was incorporated into the NorHA using light-mediated thiol-norbornene chemistry. [22] The cells were extracted to cell media through centrifugation using 25% w/w 1H,1H,2H,2H-perfluorodecanol (PFD).

All extraction was performed in a centrifuge at 200 g for 3 minutes. The continuous phase consists of 1% w/w biocompatible fluorosurfactant (RAN Biotechnology, MA) in fluorinated oil (3M Novec Engineering HFE7500).

Rheological measurement

NorHA gel precursor solution contained 1.2% NorHA with 0.8 ratio of dithiothreitol (DTT) and 0.2% (w/v) water soluble photoinitiator LAP was transferred to syringes with their tips removed, covered with a cover slip, and irradiated with UV light (10 mW/cm^2, 365nm) for 5 seconds. NorHA gels were incubated with PBS overnight before mechanical testing. Mechanical properties of the hydrogels were tested using TA Instruments Discovery HR-2 rheometer. Oscillatory time sweeps were performed on three samples (n = 3) at a strain of 0.64% and a frequency of 1 Hz to measure the storage modulus (G') and loss modulus (G"). The Young's Modulus (substrate elasticity) was calculated following $E = 2G'(1+\nu)$ using an average Poisson's ratio (ν) of 0.5. [27,28]

Results and discussions:

"Tip streaming" mode of AC electrospray

With appropriate back pressure and a DC (direct current) electric potential applied across a liquid interface, the interface becomes charged and form a sharp conic structure with a 49 degree half angle (Taylor cone).[29] Despite earlier attempts to exploit the sharp conic structure to encapsulate cells, [30–32] multiple cells are encapsulated in a single droplet, which is often attributed to recirculation within the Taylor cone. [33] However, a recent discovery in our lab shows that an AC field can produce a much sharper cone (11 degrees) due to dielectric polarization, rather than the direct ion charging of the DC cone.[34] This slender AC cone cannot sustain a recirculation flow and ejects electroneutral droplets much larger than the charged droplets of DC Taylor cone. Following our earlier jargon,[23] we define such droplet generation from the AC cone as "tip streaming" (Figure 1A). Stable AC cone and tip streaming only occurs at frequencies beyond the inverse charge relaxation time of the orifice $D/\lambda R \sim 10$ kHz, where D is the diffusivity of the dominant ion such as Calcium (~10^{-5} cm^2/s), λ is the Debye length of the cell solution (~few nm for the typical cell medium in

the dispersed phase) and R ~ 20 microns the orifice radius. The choice of the frequency should also avoid field penetration into the cell beyond megahertz.[35] Here, we report the first successful encapsulation of the cells with the tip streaming mode of the AC cone at an alternating frequency of 300 kHz.

Consistent with our previous observations, at low frequencies below the inverse charge relaxation time of 10 kHz, a DC Taylor cone is still observed.[36,37] An incoming cell often fails to block the flow supplying the tip streaming and starts to recirculate within the conic area until enough cells aggregate at the tip. The aggregated cells are eventually ejected collectively in a single droplet, as shown in Figure 1B. This multi-cell encapsulation phenomenon is consistent with earlier findings with DC sprays.[31,38] The broad Taylor cone at low frequencies evolves into the slender AC cone at frequencies higher than the inverse charge relaxation time[34] and each cell is packed into a cone apex without recirculating (Figure 1B and Movie S1). Since the tip of the AC cone has a diameter much smaller than the cell, the flow is essentially blocked by this cell at the cone apex and the trailing cells can no longer advance. The apex then pinches off to generate a droplet containing a single cell, while multiple cells may exist in the trailing conic region. There is hence a gating action much like a ball check valve in a funnel.

Conformal single-cell hydrogels coating

In order to minimize the effect of the electric field on the cells we chose the voltage potential at the lower end for tip streaming which is found to be around 420 V for 300 kHz. Appropriate applied pressure is chosen to ensure both the formation of the streaming cone and a high flow rate. It is found when the applied pressure is higher than a critical pressure 2.4 kPa, dripping droplets with 30 microns to 40 microns in diameter are created. Therefore, the applied pressure is set slightly below the critical pressure at 1.6–2.2 kPa. During tip streaming, tiny liquid droplets which have size range between one to ten microns are emitted from the cone apex as shown in Figure 1B. When no cells are present near the cone, tip streaming has a flow rate of about 5 nL/min (estimated based on the cell moving speed in the pipette) for the chosen parameters described above. The cells are emitted at a frequency of ~100 Hz. It is important to note that we did not characterize the droplet generation frequency for the tiny tip streaming droplets as they are often below the diffraction limit.

After dispersing the cells, the hydrogel layer is crosslinked by different methods depending on the hydrogel materials, as shown in Figure 1A. For crosslinking alginate and collagen gels, we used acetic acid and heat incubation respectively. On the other hand, NorHA precursor solution was crosslinked using irradiation with ultraviolet (UV) light (10 mW/cm^2, 365nm) for 5 seconds.[21,39] In order to ensure that the cell is completely encapsulated by the hydrogel layer after crosslinking process, the emulsion is first placed in an orbital shaker at 1,000 rpm for two minutes to drive the cell closer to the center of the droplet without affecting droplet monodispersity. [18] Immediately after shaking the droplets, the alginate droplets are crosslinked by adding 0.01% v/v acetic acid to the oil for two minutes [26] and the collagen droplets are gelled by incubation at 37 °C for 30 minutes.

Extraction of the droplets into cell medium is achieved by centrifugation after adding cell medium to the centrifuge tube containing the emulsion. During extraction, the interfacial

tension between the cell medium and oil phase is reduced by using 1H,1H,2H,2H-perfluorooctanol (PFO) for alginate and collagen. Most empty droplets generated from “tip streaming” are more than ten times smaller than the encapsulated single-cell particle in volume, thus the majority of them can be left in the oil phase by choosing a proper concentration of PFO that allows the larger cell-encapsulated beads to cross over the water/oil interface but not the smaller streaming droplets.

Characterization of encapsulated cells

Visualization of the microgels was done using FITC-labeled alginate and NHS-FITC dye to label the primary amine group in the collagen gel (Figure 2A–C). It is found that using PFO concentration of 10% w/w allows extraction of most cell-encapsulated alginate and collagen beads but left most small empty particles in the oil phase, as shown in Figure 2A and B. While keeping the centrifugal force and time the same, significant amount of empty alginate gel particles from streaming droplets are extracted using 20% w/w PFO as shown in Figure 2C and Figure S1A. At the same centrifugation force, we demonstrate sorting of cell loaded droplets by controlling the interfacial tension and increasing the single cell laden droplet percentage from 30% to more than 80% as shown in Figure 2E and Figure S1A. However, it is important to note that 20% w/w PFO was not sufficient to break the interfacial surface tension between NorHA microgel and the oil (Figure S1A). Instead, using 25% of 1H,1H,2H,2H-perfluordecanol (PFD) allowed extraction of 81% single cell laden microgel from the water oil emulsion (Figure 2D and E), whereas using 10% PFD (data not shown) did not allow extraction of any cell laden microgels from oil phase. We suspect that the difference in interfacial surface tension allows us to isolate these microgels with different types of perfluorocarbon liquids.

To further characterize the single-cell encapsulated microgels, their morphologies are studied using light and fluorescent microscopy techniques. Representative images of alginate, collagen, and NorHA encapsulated MDA-MB-231 cells are shown in Figure 3A, C and E respectively. The lighter green area indicates the volume of the cell and the darker green area indicates the hydrogel layer of alginate and collagen gels. NorHA microgels, on the other hand are modified with thiol-dyes to indicate the hydrogel layer in red and the volume of the cell in green. [21,39]

Thirty randomly chosen single-cell beads are analyzed for each case. For each single-cell bead, the minimum thickness t_{min} and the maximum thickness t_{max} of the gel layer can be measured as shown by the bars in Figure 3B, D and F. The average thickness of the hydrogel layer is taken by the average of the t_{min} and t_{max}. The alginate, collagen and NorHA encapsulated hydrogel beads have average thickness of 4.4 ± 0.8, 4.1 ± 2.0 and 2.85 ± 1 μm, respectively. To better evaluate how close the cell is placed to the center of the gel bead, concentric index (CI) is defined as:

$$CI = \frac{t_{\max} - t_{\min}}{t_{\max} + t_{\min}}$$

When the cell is placed at the most center of the bead, CI equals to zero; when the cell is placed at the edge of the bead, CI equals to one. If an arbitrary value of CI of 0.8 is used to classify the single-cell beads into centered and off-centered groups, more than 86% beads are centered, as shown in Figure 3B, D and F.

The viability of the MDA-MB-231 cells are studied using Live/Dead cell viability assay. Cell viability immediately after microgel encapsulation was 88.25± 6.63% and 93.14± 2.65% for alginate and collagen respectively. The viability remained 82.97± 0.9% and 73.81± 5.14% after 24 hours *in vitro* for alginate and collagen encapsulated cells respectively. We did not observe cell proliferation within the microgels following cell encapsulation, which is consistent with previous reports using high molecular weight alginate gels.[10] Since NorHA gel is polymerized using free radical polymerization, photo-initiator (e.g., LAP) concentration plays an important role in cell viability. [40] The free radicals generated by the UV dosage may affect cell viability, unless they are all consumed in a reaction. Higher LAP concentration leads to faster gelation kinetics, but the excessive free radicals formed causes detrimental effect on cells. The viability of cells immediately after spray was studied using two photo-initiator concentration 0.2%(w/v) and 0.3%(w/v) for the same UV exposure (10 mW/cm^2, 365nm, 5 seconds) as shown in Figure S1B. The 0.3% (w/v) LAP concentration showed less than 60% cell viability while 0.2% (w/v) showed more than 84% cell viability immediately after cell encapsulation. The optimized LAP concentration was used to obtain 89.75± 8.01% cell viability immediately after encapsulation and more than 80% of the cells are alive after 24 hours *in vitro* for NorHA microgel as shown in Figure 3H.

Differentiation potential of encapsulated hMSCs

Since hyaluronic acid hydrogels have been previously shown to support self-renewal of stem cells, tissue morphogenesis, and angiogenesis,[25,27,28,41–43] we focus our next investigation using NorHA hydrogels to encapsulate hMSCs and to study their differentiation potential. We first encapsulated single hMSCs in a thin layer of NorHA microgel having an average thickness of 4.0 ± 1.8 μm as shown Figure 4A and B. Next, we demonstrated that the encapsulated hMSCs remains more than 80% viable for three consecutive days as shown in Figure 4C. Furthermore, in order to evaluate their differentiation potential, the encapsulated hMSCs were cultured in either osteogenic or adipogenic differentiation medium. For osteogenic differentiation, calcium deposits were detected by Alizarin Red S staining in both adherent and encapsulated cells (cultured in Osteogenic differentiation medium), which are significantly different from control cells maintained in growth medium (Figure 4D and Figure S2). It is important to note that control hMSCs maintained in growth medium do not stain positive for the Alizarin Red S, which may suggest that the Alizarin Red S does not demonstrate non-specific binding to the NorHA hydrogels (Figure S2). More importantly, we did not observe a significant difference in the osteogenic differentiation potential between the encapsulated cells (58.34 ± 12.40 %) and adherent cells (50.26 ± 14.76 %) as shown in Figure 4E. For adipogenic differentiation, lipid droplets were also detected in both adherent and encapsulated cells, which were cultured in adipogenic differentiation medium as shown in Figure 4F and Figure S2. There is no significant difference in the adipogenic differentiation potential between the adherent and encapsulated cells (Figure 4G). These

observations are consistent with previous studies that suggest HA hydrogels with a moderate elastic modulus (2.86 ± 0.02 kPa; Figure S3) and cultured in the appropriate differentiation medium can support the osteogenic and adipogenic differentiation of hMSCs.[20,44,45]

We chose NorHA condition with fixed rheological and mechanical properties (Figure S3) to demonstrate the feasibility of our novel technology to support the viability and differentiation potential of hMSCs. However, this unique technology can be broadly applied to other type of hydrogels with tunable mechanics, through either covalent or physical crosslinking, to enable precise controlled over stem cell differentiation. [46–48] Moreover, these microgels containing cells can be used as versatile bio-inks for various 3D printing applications,[39,49–51] as well as building blocks for annealed particles hydrogels and granular hydrogels for regenerative medicine.[52–54] Collectively, we show that the encapsulated hMSCs within NorHA microgel using our novel platform remain in high viability and preserve their robust differentiation potential, which could pave the way for a variety of applications from fundamental stem cell biology research to developing therapeutic cell-based therapy.

Conclusions

In conclusion, we demonstrate a single-cell encapsulation method based on immersed AC electrospray that is compatible with traditional crosslinking strategies for both natural and synthetic hydrogels. Using the “tip streaming” mode, cells are ejected as they block the streaming flow of the alginate, collagen, or NorHA precursor solution resulting in a hydrogel droplet with a single cell. Alternating frequency higher than the charge relaxation frequency of the precursor solution is shown to be able to generate slender cones that help avoid cell aggregation within the conic meniscus. After crosslinking, the smaller empty particles can be separated from the single-cell particles using moderate extraction condition resulting in predominant single cell particles in cell media (>80%). The final gel layer around the cell has a typical thickness of around four microns allowing fast nutrient transport and better cell survival. Thanks to the common electrospray behavior that exists in many solution types, we envision that such a technology can be applicable to various cell types and hydrogel systems, such as photo-crosslinked [47,55] and dynamic hydrogels [46,56,57]. Since microgels fabrication technique can influence the properties of granular hydrogels,[54] this high-throughput single-cell encapsulation technique can be used to generate microgels with tunable properties as building blocks for granular hydrogels.[58] Collectively, this unique technology has the potential to make high impact contribution in a range of applications in cell therapy, pharmacokinetic screening, and regenerative medicine.

Supplementary Material

Refer to Web version on PubMed Central for supplementary material.

Acknowledgments

Z.P., V.Y. and H.-C.C. acknowledge the support of NIH Grant R21-HG009010–01 and The C. Moschetto Discovery Fund. L.B., F.F., and D.H-P acknowledge support from the University of Notre Dame through “Advancing our Vision” initiative, the Harper Cancer Research Institute –American Cancer Society Institutional Research Grant

(IRG-17–182-04), and Career Development Award (19CDA34630012) from the American Heart Association (AHA).

Notes and references

1. Kamperman T, Karperien M, Le Gac S. and Leijten J, Trends Biotechnol., 2018, 36, 850–865. [PubMed: 29656795]
2. Matuła K, Rivello F. and Huck WTS, Adv. Biosyst, 2020, 4, 1900188.
3. Terekhov SS, V Smirnov I, V Stepanova A, V Bobik T, Mokrushina YA, Ponomarenko NA, Belogurov AA, Rubtsova MP, V Kartseva O, Gomzikova MO, Moskovtsev AA, Bukatin AS, V Dubina M, Kostryukova ES, V Babenko V, Vakhitova MT, Manolov AI, V Malakhova M, Kornienko MA, V Tyakht A, Vanyushkina AA, Ilina EN, Masson P, Gabibov AG and Altman S, Proc. Natl. Acad. Sci, 2017, 114, 2550 LP –2555. [PubMed: 28202731]
4. Mao AS, Özkale B, Shah NJ, Vining KH, Descombes T, Zhang L, Tringides CM, Wong S-W, Shin J-W, Scadden DT, Weitz DA and Mooney DJ, Proc. Natl. Acad. Sci. U. S. A, 2019, 116, 15392–15397.
5. Kamperman T, Henke S, Visser CW, Karperien M. and Leijten J, Small, 2017, 13, 1603711.
6. de Rutte JM, Koh J. and Di Carlo D, Adv. Funct. Mater, 2019, 29, 1900071.
7. Oh B, Swaminathan V, Malkovskiy A, Santhanam S, McConnell K. and George PM, Adv. Sci, 2020, 7, 1902573.
8. Wilson JT, Cui W, Kozlovskaya V, Kharlampieva E, Pan D, Qu Z, Krishnamurthy VR, Mets J, Kumar V, Wen J, Song Y, V Tsukruk V. and Chaikof EL, J. Am. Chem. Soc, 2011, 133, 7054–7064. [PubMed: 21491937]
9. Veiseh O, Doloff JC, Ma M, Vegas AJ, Tam HH, Bader AR, Li J, Langan E, Wyckoff J, Loo WS, Jhunjhunwala S, Chiu A, Siebert S, Tang K, Hollister-Lock J, Aresta-Dasilva S, Bochenek M, Mendoza-Elias J, Wang Y, Qi M, Lavin DM, Chen M, Dholakia N, Thakrar R, Lacík I, Weir GC, Oberholzer J, Greiner DL, Langer R. and Anderson DG, Nat. Mater, 2015, 14, 643. [PubMed: 25985456]
10. Mao AS, Shin J-W, Utech S, Wang H, Uzun O, Li W, Cooper M, Hu Y, Zhang L, Weitz DA and Mooney DJ, Nat. Mater, 2016, 16, 236. [PubMed: 27798621]
11. Visser CW, Kamperman T, Karbaat LP, Lohse D. and Karperien M, Sci. Adv, 2018, 4, eaao1175.
12. Xu T, Kincaid H, Atala A. and Yoo JJ, J. Manuf. Sci. Eng, , DOI:10.1115/1.2903064.
13. Kamalakshakurup G. and Lee AP, Lab. Chip, 2017, 17, 4324–4333. [PubMed: 29138790]
14. Schoeman RM, Kemna EWM, Wolbers F. and van den Berg A, ELECTROPHORESIS, 2014, 35, 385–392. [PubMed: 23856757]
15. Tomei AA, Manzoli V, Fraker CA, Giraldo J, Velluto D, Najjar M, Pileggi A, Molano RD, Ricordi C, Stabler CL and Hubbell JA, Proc. Natl. Acad. Sci, 2014, 111, 10514 LP –10519.
16. Headen DM, García JR and García AJ, Microsyst. Nanoeng, 2018, 4, 17076.
17. Dhar M, Lam JN, Walser T, Dubinett SM, Rettig MB and Di Carlo D, Proc. Natl. Acad. Sci, 2018, 115, 9986 LP –9991. [PubMed: 30224472]
18. Lienemann PS, Rossow T, Mao AS, Vallmajo-Martin Q, Ehrbar M. and Mooney DJ, Lab. Chip, 2017, 17, 727–737. [PubMed: 28154867]
19. Kusuma S, Shen Y-I, Hanjaya-Putra D, Mali P, Cheng L. and Gerecht S, Proc. Natl. Acad. Sci, 2013, 110, 12601–12606.
20. Huebsch N, Lippens E, Lee K, Mehta M, Koshy ST, Darnell MC, Desai RM, Madl CM, Xu M, Zhao X, Chaudhuri O, Verbeke C, Kim WS, Alim K, Mammoto A, Ingber DE, Duda GN and Mooney DJ, Nat. Mater, 2015, 14, 1269–1277. [PubMed: 26366848]
21. Vega SL, Kwon MY, Song KH, Wang C, Mauck RL, Han L. and Burdick JA, Nat. Commun, 2018, 9, 614. [PubMed: 29426836]
22. Gramlich WM, Kim IL and Burdick JA, Biomaterials, 2013, 34, 9803–9811. [PubMed: 24060422]
23. Pan Z, Men Y, Senapati S. and Chang H-C, Biomicrofluidics, 2018, 12, 044113.
24. Pan Z. and Chang H-C, Phys. Rev. Fluids, 2019, 4, 101701.

25. Hanjaya-Putra D, Bose V, Shen Y-I, Yee J, Khetan S, Fox-Talbot K, Steenbergen C, Burdick JA and Gerecht S, Blood, 2011, 118, 804 LP –815. [PubMed: 21527523]
26. Utech S, Prodanovic R, Mao AS, Ostafe R, Mooney DJ and Weitz DA, Adv. Healthc. Mater, 2015, 4, 1628–1633. [PubMed: 26039892]
27. Hanjaya-Putra D, Yee J, Ceci D, Truitt R, Yee D. and Gerecht S, J. Cell. Mol. Med, 2010, 14, 2436–2447. [PubMed: 19968735]
28. L Alderfer L, Russo E, Archilla A, Coe B, Hanjaya-Putra D, The FASEB Journal, 2021, 00, e21498.
29. Ingram TG, Proc. R. Soc. Lond. Ser. Math. Phys. Sci, 1964, 280, 383–397.
30. Jayasinghe SN, Qureshi AN and Eagles PAM, Small, 2006, 2, 216–219. [PubMed: 17193023]
31. Abeyewickreme A, Kwok A, McEwan JR and Jayasinghe SN, Integr. Biol, 2009, 1, 260–266.
32. Zhao S, Agarwal P, Rao W, Huang H, Zhang R, Liu Z, Yu J, Weisleder N, Zhang W. and He X, Integr. Biol. U. K, 2014, 6, 874–884.
33. Gañán-calvo AM, López-herrera JM, Herrada MA, Ramos A. and Montanero JM, J. Aerosol Sci, 2018, 125, 32–56.
34. Chetwani N, Maheshwari S. and Chang H-C, Phys. Rev. Lett, 2008, 101, 204501.
35. Gordon JE, Gagnon Z. and Chang H-C, Biomicrofluidics, 2007, 1, 044102.
36. Maheshwari S. and Chang H-C, Appl. Phys. Lett, 2006, 89, 234103.
37. Maheshwari S. and Chang H-C, J. Appl. Phys, 2007, 102, 034902.
38. Ward E, Chan E, Gustafsson K. and Jayasinghe SN, The Analyst, 2010, 135, 1042. [PubMed: 20419255]
39. Hanjaya-Putra D, Wong KT, Hirotsu K, Khetan S, Burdick JA and Gerecht S, Biomaterials, 2012, 33, 6123–6131. [PubMed: 22672833]
40. Xia B, Krutkramelis K. and Oakey J, Biomacromolecules, 2016, 17, 2459–2465. [PubMed: 27285343]
41. Gerecht S, Burdick JA, Ferreira LS, Townsend SA, Langer R. and Vunjak-Novakovic G, Proc. Natl. Acad. Sci, 2007, 104, 11298 LP –11303.
42. Wolf KJ and Kumar S, ACS Biomater. Sci. Eng, 2019, 5, 3753–3765. [PubMed: 31598545]
43. Burdick JA and Prestwich GD, Adv. Mater, 2011, 23, H41–H56. [PubMed: 21394792]
44. Khetan S, Guvendiren M, Legant WR, Cohen DM, Chen CS and Burdick JA, Nat. Mater, 2013, 12, 458–465. [PubMed: 23524375]
45. Guvendiren M. and Burdick JA, Nat. Commun, 2012, 3, 792. [PubMed: 22531177]
46. Zou L, Braegelman AS and Webber MJ, ACS Appl. Mater. Interfaces, 2019, 11, 5695–5700. [PubMed: 30707553]
47. Khetan S, Katz JS and Burdick JA, Soft Matter, 2009, 5, 1601–1606.
48. Chaudhuri O, Gu L, Klumpers D, Darnell M, Bencherif SA, Weaver JC, Huebsch N, Lee HP, Lippens E, Duda GN and Mooney DJ, Nat. Mater, 2016, 15, 326-+.
49. Highley CB, Song KH, Daly AC and Burdick JA, Adv. Sci. Weinh. Baden-Wurtt. Ger, 2018, 6, 1801076.
50. Skylar-Scott MA, Uzel SGM, Nam LL, Ahrens JH, Truby RL, Damaraju S. and Lewis JA, Sci. Adv, 2019, 5, eaaw2459.
51. Lee A, Hudson AR, Shiwarski DJ, Tashman JW, Hinton TJ, Yerneni S, Bliley JM, Campbell PG and Feinberg AW, Science, 2019, 365, 482–487. [PubMed: 31371612]
52. Griffin DR, Archang MM, Kuan C-H, Weaver WM, Weinstein JS, Feng AC, Ruccia A, Sideris E, Ragkousis V, Koh J, Plikus MV, Di Carlo D, Segura T. and Scumpia PO, Nat. Mater, 2020, 1–10. [PubMed: 31853035]
53. Darling NJ, Xi W, Sideris E, Anderson AR, Pong C, Carmichael ST and Segura T, Adv. Healthc. Mater, 2020, 9, 1901391.
54. Muir VG, Qazi TH, Shan J, Groll J. and Burdick JA, ACS Biomater. Sci. Eng,2021
55. Hanjaya-Putra D, Wong KT, Hirotsu K, Khetan S, Burdick JA and Gerecht S, Biomaterials, 2012, 33, 6123–6131. [PubMed: 22672833]

56. Hui E, Gimeno KI, Guan G. and Caliari SR, Biomacromolecules, 2019, 20, 4126–4134. [PubMed: 31600072]
57. Wei Z, Schnellmann R, Pruitt HC and Gerecht S, Cell Stem Cell, 2020, 27, 798–812.e6.
58. Gazi TH, Burdick JA, Biomaterials and Biosystems,2021;1: 100008.doi:10.1016/j.bbiosy.2021.100008

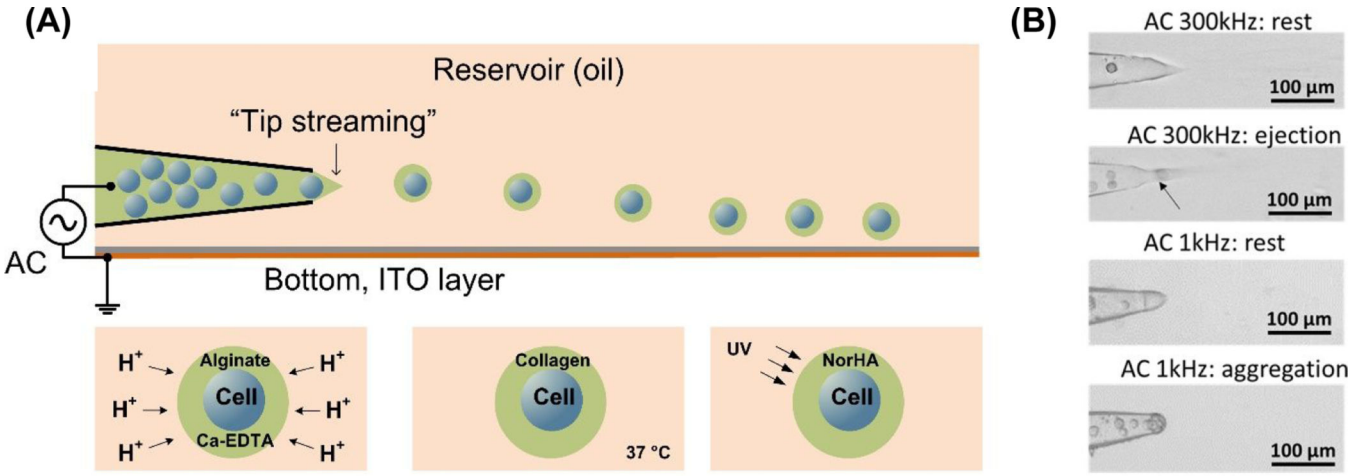

Figure 1.

(**A**) Schematic for single-cell gel coating using the tip-streaming mode. For encapsulation with alginate gel, the alginate solution is cross-linked by releasing of premixed Ca-EDTA complex using acetic acid. For encapsulation with collagen gel, the droplets were incubated at 37 °C for 30 minutes to induce gelation. Encapsulation of NorHA hydrogel was performed by photo-crosslinking of the NorHA precursor solution with UV exposure (10 mW/cm^2, 365 nm). (**B**) Snapshots of an MDA-MB-231 cell being ejected through "tip streaming" in alginate solution at high (300kHz) and low (1kHz) frequency.

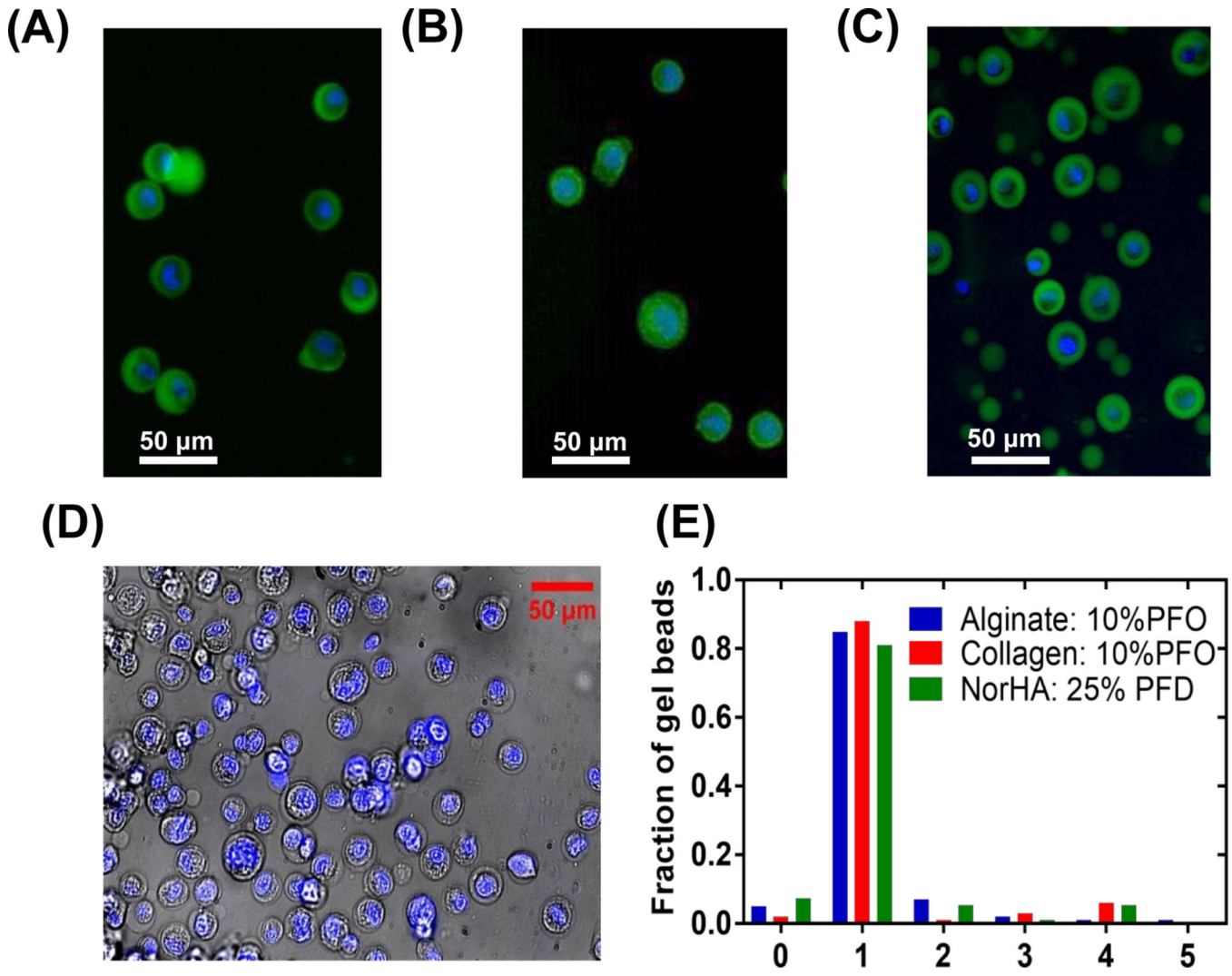

Figure 2.

(**A**) MDA-MB-231 cells encapsulated in alginate gel. Green: alginate gel; Blue: cell nucleus. (**B**) MDA-MB-231 cells encapsulated collagen in gel. Green: collagen gel; Blue: cell nucleus. (**C**) Alginate gel particles extracted using 20% w/w PFO including both empty streaming droplets and encapsulated cells. Green: alginate gel; Blue: cell nucleus. (**D**) MDA-MB-231 cells encapsulated in NorHA microgels extracted using 25% w/w PFD including both empty streaming droplets and encapsulated cells. Blue: cell nucleus. Scale bars are 50 μm. (**E**) Fraction of cells encapsulated cells per microgel bead.

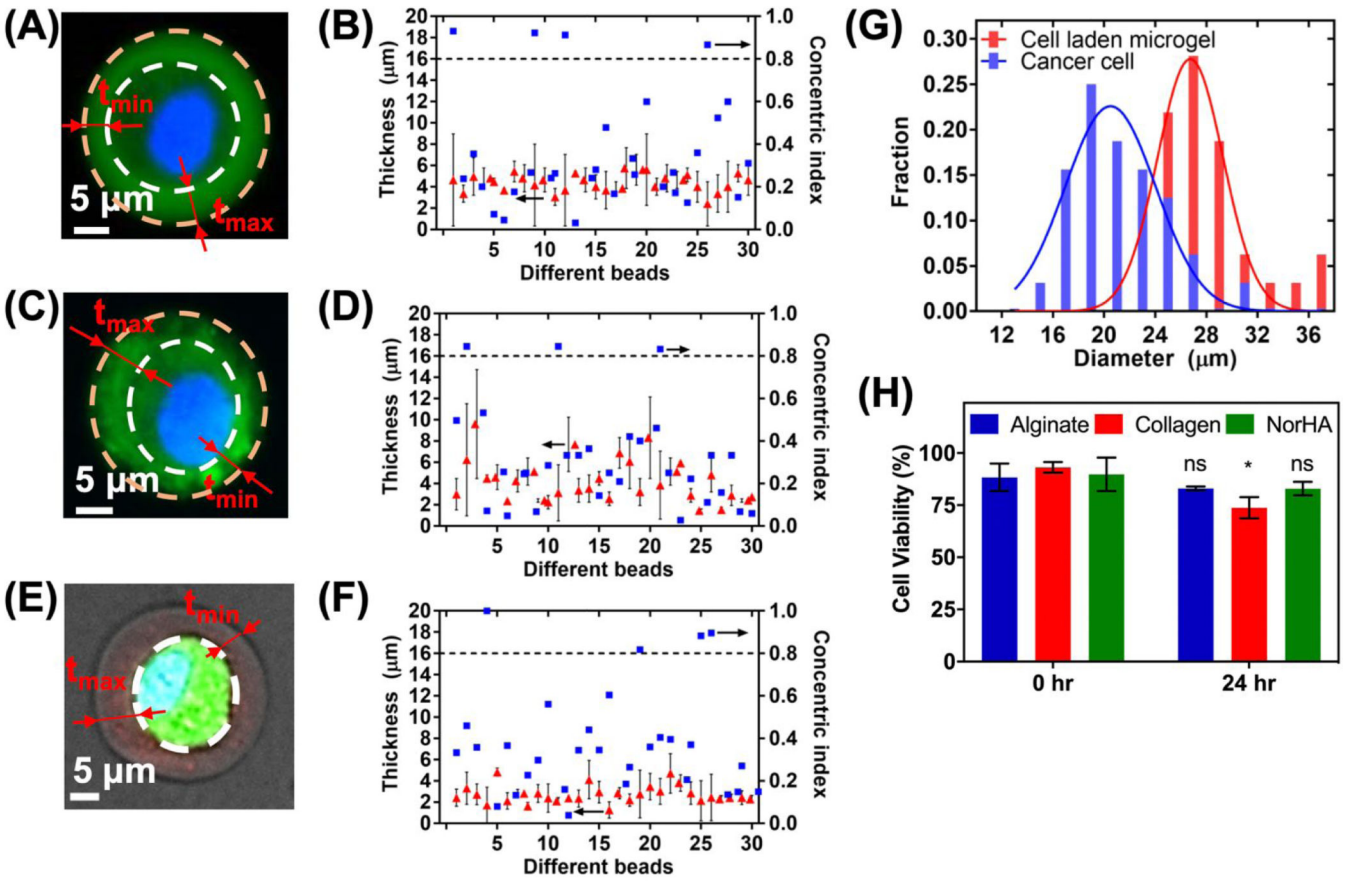

Figure 3.

(**A**) Representative image of a MDA-MB-231 cell encapsulated in alginate gel particle. The cell occupies the middle region of the bead with lighter fluorescent intensity. White dashed lines delineate cell boundaries. (**B**) Gel layer thickness (red triangle) and concentric index (blue square) of 30 randomly chosen single-cell-encapsulated alginate gel particles. (**C**) Representative image of a MDA-MB-231 cell encapsulated in collagen gel particle. (**D**) Gel layer thickness (red triangle) and concentric index (blue square) of 30 randomly chosen single-cell-encapsulated collagen gel particles (**E**) Representative image of a MDA-MB-231 cell encapsulated in NorHA gel particle. (**F**) Gel layer thickness (red triangle) and concentric index (blue square) of 30 randomly chosen single-cell-encapsulated NorHA gel particles (**G**) Distribution of microgels and cells from (**F**) depicting conformal coating (**H**) Viability of single cells encapsulated in alginate or collagen particles right after encapsulation and after 24 hours. Pair sample t test P-values =0.32, 0.028 and 0.15 for alginate, collagen and NorHA encapsulated cells, respectively.

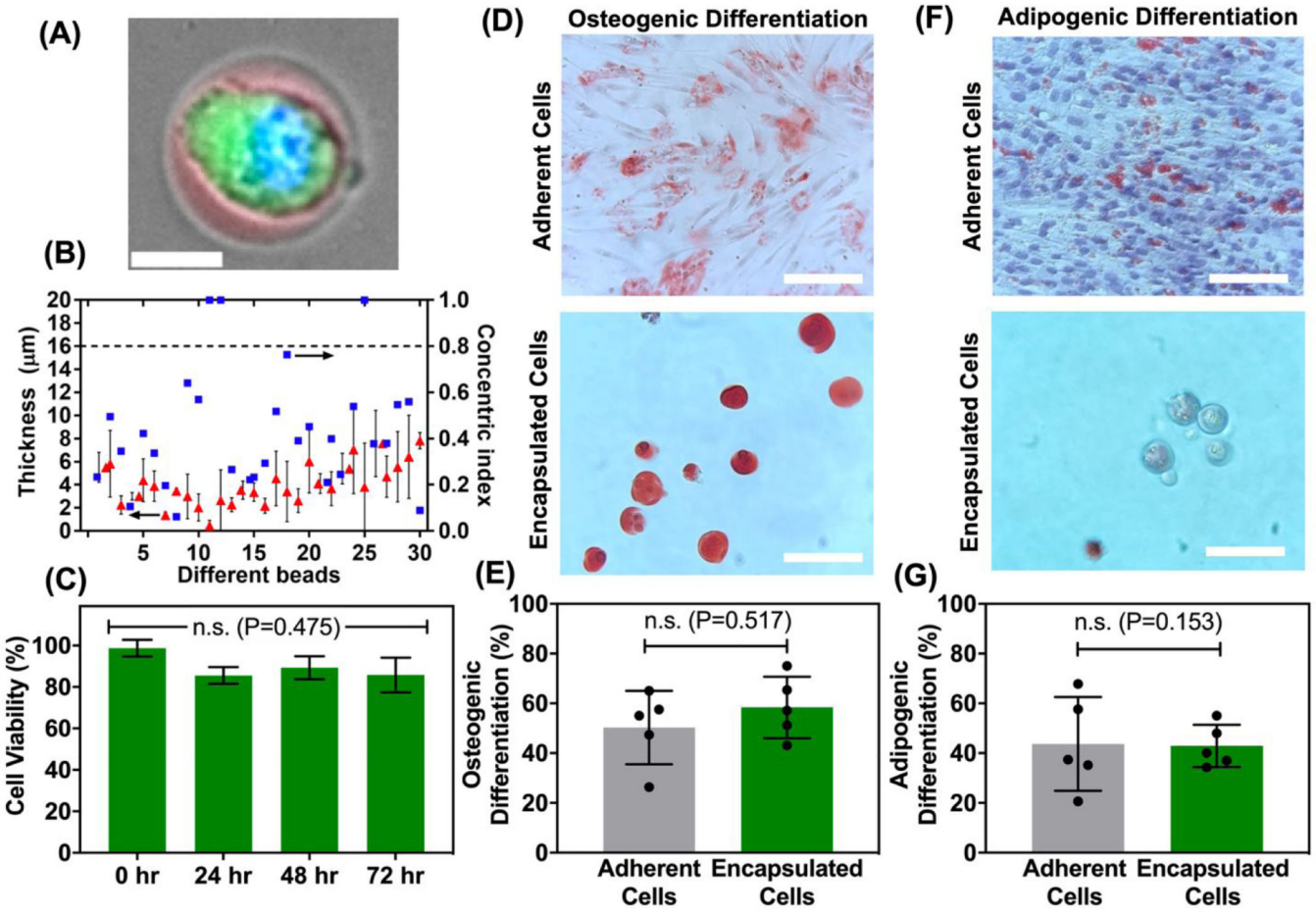

Figure 4. Human MSCs encapsulation and differentiation within NorHA microgel.

(**A**) Representative image of hMSCs encapsulated in NorHA microgel with fluorescence image superimposed with bright field image. (Blue: cell nucleus, Green: Calcein stain). Scale bar: 20μm. (**B**) Gel layer thickness (red triangle) and concentric index (blue square) of 30 randomly chosen single hMSC encapsulated NorHA gel particles. (**C**) Viability of encapsulated cells 1 day, 2 days, and 3 days after encapsulation. Data represents mean ± stdev. of five experimental run. (**D**) Microscopic images of osteogenic differentiation of hMSCs (adherent and NorHA-encapsulated cells). Differentiated cells, cultured in MSC osteogenic differentiation medium for 7 days, show calcium deposits (bright orange-red, top) as stained with Alizarin Red S solution. Scale bars are 100 μm (**E**) Quantification graph compares percentage of positive differentiated encapsulated cells versus adherent cells. P-value = 0.517. (**E**) Microscopic images of adipogenic differentiation of hMSCs (adherent and NorHA-encapsulated cells). Differentiated cells, cultured in MSC adipogenic differentiation medium for 7 days, show lipid deposits as stained with Oil Red O solution. Scale bars are 100μm (**G**) Quantification graph compares percentage of positive differentiated encapsulated cells versus adherent cells. P-value = 0.153. Data represents mean ± stdev. of five experimental runs with ≤ 30 microgels of cells analysed per condition in each replicate run.